

Phase Stability Analysis of Volume-preserving Algorithms for Accurate Single Particle Orbit Simulations in Tokamak Plasmas

Jian Wang^{*1,2}, Xiaodong Zhang¹, Lei Ye¹, and Xingyuan Xu¹

¹*Institute of Plasma Physics, Hefei Institutes of Physical Science, Chinese Academy of Science, Hefei 230031, China*

²*University of Science and Technology of China, Hefei 230026, China*

Abstract

Second-order Volume-preserving algorithms (VPAs) for simulating charged particle motion in electromagnetic fields have been generalized to a rotating angle formulation by using the matrix decomposition methods. Based on this method, the phase stability of this class of VPAs has been analyzed by using the Discrete Fourier Transformations (DFT) technique. It is found that two prominent VPAs, namely the G_h^2 and the Boris algorithm, exhibit optimal phase precision for high-frequency (gyro motion) and low-frequency dynamics (transit/bounce motion), respectively. These findings have been empirically verified through numerical experiments. The insights gained from this study enable the selection of an appropriate VPA for practical simulations based on the characteristic frequencies of specific physics problems, which can substantially enhance numerical accuracy and improve computational efficiency for long-term simulations.

Keywords: charged particle dynamics, volume-preserving algorithms, Discrete Fourier Transformations, phase stability, full kinetic simulations

1 Introduction

Numerical simulation of the trajectory of a charged particle in a tokamak is a fundamental problem with significant importance within the field. On one hand, understanding the behavior of individual particles in specific electromagnetic fields can elucidate numerous key physics phenomena. On the other hand, the aggregation of single-particle orbits lays the groundwork for first-principle, self-consistent large-scale numerical simulations, such as in various particle-in-cell (PIC) [1, 2] and semi-Lagrangian (SL) [3] codes.

*Corresponding Author. Email address: wang.jian@ipp.ac.cn

The motion of a charged particle in tokamak plasma consist of a fast gyro-motion and a slow drift-motion of the gyro-center. For low frequency problems with $\omega \ll \omega_c$, such as drift-waves and shear Alfvén waves, it is sufficient to employ the gyrokinetic model [4] and trace the gyro-center trajectory by averaging out the gyro-angle, reducing the particle dynamics from 6D to 5D. Here, ω and ω_c represent the characteristic frequency of waves and gyro-motion, respectively. However, for the problems with $\omega \geq \omega_c$, such as radio frequency (RF) waves [5, 6], high-frequency turbulence [7] and ion cyclotron emission (ICE) [8], the full kinetic model must be utilized, which requires the computation of the full orbit of particles. Moreover, in the gyrokinetic simulations of edge/pedestal plasma, there has also been a paradigm shift towards utilizing full kinetic ions in place of gyrokinetic ions [9, 10]. This approach significantly extends the applicability of the numerical models across a broader spectrum of time-space scales.

The Boris algorithm [11–13] has become the de facto standard of the explicit integration schemes for calculating the full particle orbits in tokamak plasma. Despite its relatively lower precision of truncation error (2nd-order accuracy, in comparison to the 4th-order Runge-Kutta scheme) in a single time step, the Boris algorithm has inherent robust conservation properties across long temporal scales [14–16], which are crucial for the numerical investigation of the multi-time-scale nature of plasma physics in tokamak. It has been pointed out that a key factor in its success is the algorithm’s ability to conserve phase space volume, essential for all Hamiltonian systems [17]. Such numerical schemes, known as Volume-Preserving Algorithms (VPAs), can be systematically derived through Lie algebraic methods [18]. Another volume-preserving algorithm, which is firstly introduced in [19] and herein referred to as G_h^2 , has also been developed by modifying the magnetic-field-induced rotation angle of particle velocity in the Boris algorithm. While G_h^2 exhibits a minor disadvantage in the accuracy of adiabatic invariant, it possesses a faster convergence rate for numerical solutions compared to the Boris algorithm in a static electromagnetic field. Besides, advanced volume-preserving methods of higher precision have been developed and applied in both non-relativistic and relativistic dynamics of charged particles [20–22]. These methods have delivered highly accurate results in long-term simulations.

Although the theoretical framework of VPAs has reached a sophisticated level, the main focus has primarily been on the conservative properties of VPAs in long-time simulations. It is known that the wave-particle resonances between charged particles and a spectrum of electromagnetic waves across different frequencies play an essential role in most physics phenomena in tokamak plasma, such as RF heating and Energetic particle (EP)-driven instabilities. Therefore, numerical precision in the particle phase in given fields is of great importance for numerical investigations of these issues. However, the phase stability of various VPAs has not been extensively explored.

In this work, VPAs for simulating charged particle motion in electromagnetic fields have been generalized to a rotating angle formulation using matrix decomposition methods. Based on this method, the phase stability of a class of VPAs has been analyzed using Discrete Fourier Transformations (DFT) technique.

The theoretical phase stability analysis presented here proves that the Boris algorithm and G_h^2 are optimally suited for computing low and high-frequency components, respectively, within this class of second-order VPAs. Numerical simulations of charged particle trajectories within a typical tokamak toroidal magnetic field have been executed to verify the analytical predictions, demonstrating different performances in calculating various scales of motion by the two representative VPAs. These new findings can enable the selection of more appropriate numerical integral schemes in constructing full particle orbits, potentially with larger time step sizes, based on the characteristic frequency of the physical problem at hand. Such selection can also substantially reduce computational time and improve the efficiency of long-term simulations.

This paper is organized as follows. Section II delineates the generalization of a series of VPAs in matrix notation. Sec.III presents the theoretical phase stability analysis of the volume-preserving algorithms across various frequencies. Compared in Sec.IV are the numerical results of the charged particle trajectories in a typical Tokamak toroidal magnetic field by the Boris algorithm and G_h^2 respectively. Finally, Sec.V concludes the paper.

2 Generalization of Volume-Preserving Algorithms

This section is dedicated to the generalization of VPAs, adhering to the definitions established in [17]. The formulation of these algorithms is articulated through matrix notation, which will facilitate the subsequent phase stability analysis.

The motion of charged particles in an electromagnetic field $\vec{E} = (E^x, E^y, E^z)^T$ and $\vec{B} = (B^x, B^y, B^z)^T$ is governed by the Lorentz-Newton equation

$$m \frac{d\vec{v}}{dt} = q(\vec{v} \times \vec{B} + \vec{E}) \quad (1.a)$$

$$\frac{d\vec{r}}{dt} = \vec{v} \quad (1.b)$$

with m the mass, q the electric charge, and $\vec{r} = (x, y, z)^T$, $\vec{v} = (v^x, v^y, v^z)^T$ the position and velocity of the charged particle under Cartesian coordinates. To facilitate the discussion, we will normalize the magnetic field \vec{B} , electric field \vec{E} , velocity variable \vec{v} , position variable \vec{r} time variable t by basic quantities

$$B_{ref} = B_0, v_{ref} = v_0 \quad (2.a)$$

with B_0 the magnetic field strength on the magnetic axis, v_0 the initial velocity magnitude of the particle. And derived quantities are given by

$$E_{ref} = B_{ref} v_{ref} = B_0 v_0, t_{ref} = \frac{m}{q B_{ref}} = \frac{m}{q B_0}, r_{ref} = v_{ref} t_{ref} = \frac{m v_0}{q B_0} \quad (2.b)$$

Replacing $\vec{B}, \vec{E}, \vec{v}, \vec{r}$ and t by $\frac{\vec{B}}{B_{ref}}, \frac{\vec{E}}{E_{ref}}, \frac{\vec{v}}{v_{ref}}, \frac{\vec{r}}{r_{ref}}$ and $\frac{t}{t_{ref}}$ in equations (1) yields

$$\frac{d\vec{v}}{dt} = \vec{v} \times \vec{B} + \vec{E} \quad (3.a)$$

$$\frac{d\vec{r}}{dt} = \vec{v} \quad (3.b)$$

Throughout the discourse in Section 2 and Section 3, we shall persistently utilize the above normalized form. The Lorentz force term $\vec{v} \times \vec{B}$ can be written in matrix form as

$$\frac{d\vec{v}}{dt} = \mathcal{B}\vec{v} + \vec{E} \quad (4.a)$$

Here, the real skew-symmetric matrix \mathcal{B} is given by

$$\mathcal{B} = \begin{bmatrix} 0 & B^z & -B^y \\ -B^z & 0 & B^x \\ B^y & -B^x & 0 \end{bmatrix} \quad (4.b)$$

Since \mathcal{B} is a real skew-symmetric matrix, it can be diagonalized by a unitary matrix P

$$\mathcal{B} = P\Lambda P^* \quad (5.a)$$

Here, the unitary matrix P and the diagonal matrix Λ are given by

$$P = \frac{1}{B} \begin{bmatrix} B^x & \frac{-B^x B^y - B^z B^i}{\sqrt{2((B^x)^2 + (B^z)^2)}} & \frac{B^x B^y - B^z B^i}{\sqrt{2((B^x)^2 + (B^z)^2)}} \\ B^y & \frac{\sqrt{(B^x)^2 + (B^z)^2}}{\sqrt{2((B^x)^2 + (B^z)^2)}} & -\frac{\sqrt{(B^x)^2 + (B^z)^2}}{\sqrt{2((B^x)^2 + (B^z)^2)}} \\ B^z & \frac{-B^y B^z + B^x B^i}{\sqrt{2((B^x)^2 + (B^z)^2)}} & \frac{B^y B^z + B^x B^i}{\sqrt{2((B^x)^2 + (B^z)^2)}} \end{bmatrix} \quad (5.b)$$

$$\Lambda = \text{diag}(0, Bi, -Bi) \quad (5.c)$$

with P^* the conjugate transpose matrix of P , $B = \sqrt{(B^x)^2 + (B^y)^2 + (B^z)^2}$ the magnetic field strength.

Now we consider the numerical integral schemes of (3). Let Δt denotes the fixed time step size, the subscript k represents variables in the k -th time step and $z_k = (\vec{r}_k, \vec{v}_k) = (\vec{r}(k + \frac{1}{2})\Delta t, \vec{v}(k\Delta t))$ denotes coordinates of the time step in phase space. The recurrence relation from z_k to z_{k+1} in numerical algorithms generates a one-step map ψ

$$\psi : z_k = (\vec{r}_k, \vec{v}_k) \rightarrow z_{k+1} = (\vec{r}_{k+1}, \vec{v}_{k+1}) \quad (6)$$

Algorithms satisfying $|\frac{\partial \psi}{\partial z_k}| = 1$ for arbitrary k conserve the phase space volume in each time step, thus are referred to as volume-preserving algorithms [17]. The well-known Boris method, as a typical example of VPA, handles the electric and magnetic forces separately

$$\vec{v}^- = \vec{v}_k + \frac{1}{2}\Delta t \cdot \vec{E}_k \quad (7.a)$$

$$\vec{v}^+ = \vec{v}^- + \frac{1}{2}\Delta t \cdot (\vec{v}^+ + \vec{v}^-) \times \vec{B}_k \quad (7.b)$$

$$\vec{v}_{k+1} = \vec{v}^+ + \frac{1}{2}\Delta t \cdot \vec{E}_k \quad (7.c)$$

$$\vec{r}_{k+1} = \vec{r}_k + \Delta t \cdot \vec{v}_{k+1} \quad (7.d)$$

with $\vec{E}_k = \vec{E}((k + \frac{1}{2}) \cdot \Delta t)$, $\vec{B}_k = \vec{B}((k + \frac{1}{2}) \cdot \Delta t)$ the electromagnetic field of the k -th time step. Equations (7) can be similarly written in matrix form as

$$\vec{v}_{k+1} = R_k^B \vec{v}_k + \frac{\Delta t}{2}(I + R_k^B)\vec{E}_k \quad (8.a)$$

$$\vec{r}_{k+1} = \vec{r}_k + \Delta t \cdot R_k^B \vec{v}_k + \frac{\Delta t^2}{2}(I + R_k^B)\vec{E}_k \quad (8.b)$$

Here, the rotation matrix of the Boris algorithm in the k -th time step R_k^B is given by

$$R_k^B = (I - \frac{\Delta t}{2}\mathcal{B}_k)^{-1}(I + \frac{\Delta t}{2}\mathcal{B}_k) \quad (8.c)$$

Substituting equations (5) into (8.c) yields

$$R_k^B = P_k \Lambda_k^B P_k^* \quad (9.a)$$

Here, the diagonal matrix Λ_k^B are given by

$$\Lambda_k^B = \text{diag}(1, \exp(\theta_k^B \cdot i), \exp(-\theta_k^B \cdot i)) \quad (9.b)$$

and $\theta_k^B = 2\arctan(\frac{1}{2}B_k \cdot \Delta t)$ is the magnetic-field-induced rotation angle of the velocity variable \vec{v}_k in the k -th time step, which satisfies the following condition of consistency

$$\lim_{\Delta t \rightarrow 0} \frac{\theta_k^B}{B_k \cdot \Delta t} = 1 \quad (9.c)$$

According to Ref. [17], the volume-preserving condition is identical to $\det(R_k^B) = 1$ for arbitrary k . Ref. [17] provides proof by the theory of Cayley transformations, while a different perspective is presented in this paper

$$\det(R_k^B) = |\det(P_k)\det(\Lambda_k^B)\det(P_k^*)| = |\det(P_k)||\det(\Lambda_k^B)||\det(P_k^*)| \quad (10)$$

Since P_k is a unitary matrix, $|\det(P_k)| = |\det(P_k^*)| = 1$. From equation (9.b), we have

$$|\det(\Lambda_k^B)| = 1 \cdot |\exp(\theta_k^B \cdot i)| \cdot |\exp(-\theta_k^B \cdot i)| = 1 \quad (11)$$

Thus $\det(R_k^B) = 1$ is easily obtained. Noted that the volume-preserving property remains valid for any other rotation angle θ_k satisfying the condition of consistency. A class of volume-preserving algorithms can therefore be easily generalized by a similar methodology.

Generalization of a class of volume-preserving algorithms. A class of volume-preserving algorithms can be derived from the following format

$$\vec{v}_{k+1} = R_k \vec{v}_k + \frac{\Delta t}{2} (I + R_k) \vec{E}_k \quad (12.a)$$

$$\vec{r}_{k+1} = \vec{r}_k + \Delta t \cdot R_k \vec{v}_k + \frac{\Delta t^2}{2} (I + R_k) \vec{E}_k \quad (12.b)$$

Here,

$$R_k = P_k \Lambda_k P_k^* \quad (12.c)$$

$$\Lambda_k = \text{diag}(1, \exp(\theta_k \cdot i), \exp(-\theta_k \cdot i)) \quad (12.d)$$

and θ_k is the magnetic-field-induced rotation angle of the velocity variable \vec{v}_k in the k -th time step, which needs to satisfy the following condition of consistency

$$\lim_{\Delta t \rightarrow 0} \frac{\theta_k}{B_k \cdot \Delta t} = 1 \quad (12.e)$$

A variety of volume-preserving algorithms can be obtained by considering various values of the magnetic-field-induced rotation angle θ as a function of the time step size Δt satisfying equation (12.e). A straightforward approach is to take $\theta = B \cdot \Delta t$. The corresponding algorithm has already been derived and is referred to as G_h^2 in [19] by Lie algebra and represented in exponential matrix form. We will consistently use G_h^2 to represent this algorithm in the subsequent text.

3 Phase Stability Analysis of VPAs in Various Frequencies

In this section, we conduct a theoretical analysis of the phase stability of the volume-preserving algorithms constructed by equations (12) across a spectrum of frequencies by the Discrete Fourier Transformations (DFT)

$$\vec{f}(\omega) = \frac{1}{N} \sum_{m=0}^{N-1} \vec{r}(t^m) \exp\left(-\frac{2\pi\omega}{T} t^m \cdot i\right), 0 \leq \omega \leq N-1 \quad (13)$$

and its inverse transformation is

$$\vec{r}(t^n) = \sum_{\omega=0}^{N-1} \vec{f}(\omega) \exp\left(\frac{2\pi\omega}{T} t^n \cdot i\right), 0 \leq n \leq N-1 \quad (14)$$

with Δt the time step size, T the total simulation time (all variables in this section remain normalized as stated in Section 2), $N = \frac{T}{\Delta t}$ the total number of time grids and $t^m = (m + \frac{1}{2}) \cdot \Delta t$ the time of position variable \vec{r} in the m -th time

step. From equation (14), the position variable \vec{r} can be interpreted as a linear combination of trigonometric functions, each with a distinct frequency $\frac{2\pi\omega}{T}$ and an associated DFT coefficient $\vec{f}(\omega)$. Since the slow-scale guiding center motions and the fast-scale cyclotron motions can be regarded as low and high frequency components of \vec{r} , the phase stability of the algorithms can be evaluated through the convergence rate of their respective DFT coefficients $\vec{f}(\omega)$ as the time step size Δt vanishes.

We make the following assumptions for further derivations

(1). The total simulation time T takes the period of the slow-scale drift motion, which is much larger than that of the cyclotron period, i.e. T is considerably large and $\frac{1}{T} = O(\epsilon)$ is considered to be an infinitesimal quantity.

(2). The influence of the electric field is excluded, namely $\vec{E} = (0, 0, 0)^T$. In the absence of the electric field, the energy is strictly preserved by volume-preserving algorithms. From equation (12.a), we have

$$\|\vec{v}_{k+1}\|_2 = \|R_k \vec{v}_k\|_2 = \|P_k \Lambda_k P_k^* \vec{v}_k\|_2 \quad (15)$$

Since P_k, Λ_k and P_k^* are all unitary matrices, their corresponding linear transformations conserve the 2-norm of vectors. Thus we have $\|\vec{v}_k\|_2 = \|\vec{v}_{k-1}\|_2 = \dots = \|\vec{v}_0\|_2 = v_0$, with v_0 the initial magnitude of velocity.

(3). The direction of the magnetic field remains unaltered, namely $\vec{B} = B(\vec{r})\vec{e}_0$, which means the corresponding unitary matrix P is held constant. The variation of the magnetic field within a single time step ΔB needs to satisfy the following condition of approximation

$$\Delta B = O(\epsilon^{1+\alpha}), \alpha > 0 \quad (16)$$

This stipulation elucidates that ΔB is an infinitesimal of a higher order compared to ϵ . Under these conditions, the numerical solutions \vec{v}^m, \vec{r}^m in the m -th time step are readily obtained

$$\vec{v}_m = \prod_{n=1}^m R_n \vec{v}_0 = P \text{diag} \left(1, \prod_{n=1}^m \lambda_{2,n}, \prod_{n=1}^m \lambda_{3,n} \right) P^* \vec{v}_0 \quad (17.a)$$

$$\vec{r}_m = \vec{r}_0 + \frac{1}{2} \vec{v}_0 \cdot \Delta t + \sum_{j=1}^m \vec{v}_j \cdot \Delta t \quad (17.b)$$

Here $\lambda_{2,n} = \exp(\theta_n \cdot i)$, $\lambda_{3,n} = \exp(-\theta_n \cdot i)$. From (13), we have

$$\vec{f}(\omega) = \frac{\Delta t}{T} \sum_{m=0}^{N-1} \vec{r}_m \exp \left(-k \left(m + \frac{1}{2} \right) \Delta t \cdot i \right) \quad (18)$$

with $k = \frac{2\pi\omega}{T}$. Substituting equations (17) into (18) yields

$$\vec{f}(\omega) = \frac{\Delta t}{T} \frac{\exp(-\frac{1}{2}k\Delta t \cdot i)}{1 - \exp(-k\Delta t \cdot i)} P \text{diag}(\lambda_1, \lambda_2, \lambda_3) P^* \vec{v}_0 \quad (19.a)$$

Given the above condition (16), $\lambda_1, \lambda_2, \lambda_3$ can be approximated as

$$\lambda_1 = -N\Delta t = -T \quad (19.b)$$

$$\lambda_2 = \left[\left(\prod_{m=2}^N \lambda_{2,m} - 1 \right) \left(\frac{\lambda_{2,1}}{1 - \lambda_{2,1}} - \frac{\lambda_{2,1} \exp(-k\Delta t \cdot i)}{1 - \lambda_{2,1} \exp(-k\Delta t \cdot i)} \right) + O(\epsilon^\alpha) \right] \Delta t \quad (19.c)$$

$$\lambda_3 = \left[\left(\prod_{m=2}^N \lambda_{3,m} - 1 \right) \left(\frac{\lambda_{3,1}}{1 - \lambda_{3,1}} - \frac{\lambda_{3,1} \exp(-k\Delta t \cdot i)}{1 - \lambda_{3,1} \exp(-k\Delta t \cdot i)} \right) + O(\epsilon^\alpha) \right] \Delta t \quad (19.d)$$

with $\lambda_{2,1}$ the initial value of $\lambda_{2,n}$, $\lambda_{3,1}$ the initial value of $\lambda_{3,n}$. See specific derivations of approximation in appendix. λ_2, λ_3 are associated with the magnetic-field-induced rotation angle θ , while the remaining variables in equations (19) are irrelevant and will therefore be disregarded in the subsequent discussions. We will exclusively concentrate on the convergence rate of λ_2 in various volume-preserving algorithms and their corresponding rotation angle θ . λ_2 can be reduced to the following form

$$\lambda_2 = \left(\prod_{m=2}^N \lambda_{2,m} - 1 \right) [h(k, \Delta t) + O(\epsilon^\alpha \Delta t)] \cdot i \quad (20.a)$$

Here, $h(k, \Delta t)$ is given by

$$h(k, \Delta t) = \left(\frac{2 \tan \frac{\theta_1}{2}}{\Delta t} \right)^{-1} - \left(\frac{2 \tan \frac{\theta_1 - k\Delta t}{2}}{\Delta t} \right)^{-1} \quad (20.b)$$

Since $(\prod_{m=2}^N \lambda_{2,m} - 1) \sim O(1)$, it does not substantially influence the convergence rate of λ_2 . Conversely, $h(k, \Delta t)$ emerges as the primary focus of our attention. Furthermore, given the periodic nature of the problem, we shall omit the time-dependent subscripts in $h(k, \Delta t)$. For the case of low frequency components associated with slow-scale guiding center motions, i.e. $\omega \sim O(1)$, we have $k = \frac{2\pi\omega}{T} \sim O(\frac{1}{T}) \sim O(\epsilon)$ and $\lim_{\Delta t \rightarrow 0} h(k, \Delta t) = 0$. Equation (20.b) is therefore reduced to

$$h(k, \Delta t) = \left(\frac{2 \tan \frac{\theta}{2}}{\Delta t} \right)^{-1} - \left(\frac{2 \tan \frac{\theta}{2} + O(\epsilon)}{\Delta t} \right)^{-1} \quad (21)$$

The rotation angle of the Boris algorithm $\theta_B = 2\arctan(\frac{1}{2}B\Delta t)$ yields

$$h_B(k, \Delta t) = \frac{1}{B^2} O(\epsilon) \quad (22)$$

Any other volume-preserving algorithm and its corresponding rotation angle satisfying equation (12.e), i.e. $\theta = 2\arctan(\frac{1}{2}B\Delta t) + c(\Delta t^2) + O(\Delta t^3)$ with

c an arbitrary constant, yields the following result by calculating the Taylor expansion of $2\tan(\frac{\theta}{2})$

$$h(k, \Delta t) = \frac{1 - 2\frac{c}{B}\Delta t + O(\Delta t^2)}{B^2}O(\epsilon) = \frac{1 + O(\Delta t)}{B^2}O(\epsilon) \quad (23)$$

Equations (22) and (23) demonstrate that the Boris algorithm exhibits the fastest convergence rate of λ_2 than other volume-preserving methods, due to the fact that it eliminates the first-order and higher-order terms of Δt in $h(k, \Delta t)$. Consequently, the Boris algorithm stands as the most effective scheme for calculating slow-scale guiding center motions within this series of volume-preserving algorithms.

Now we consider the case of large ω related to fast scale cyclotron motions, i.e. $\omega = B \cdot \frac{T}{2\pi}$ and $k = \frac{2\pi\omega}{T} = B$ and $\lim_{\Delta t \rightarrow 0} \frac{1}{h(k, \Delta t)} = 0$. Similarly, the rotation angle of G_h^2 , i.e. $\theta_{G_h^2} = B\Delta t$ yields

$$\frac{1}{h_{G_h^2}(k, \Delta t)} = 0 \quad (24)$$

Any other volume-preserving algorithm and its corresponding rotation angle satisfying equation (12.e), i.e. $\theta = B\Delta t + c(\Delta t^2) + O(\Delta t^3)$ with c an arbitrary constant, yields the following result by similarly calculating the Taylor expansion of $2\tan\frac{\theta - k\Delta t}{2}$

$$\frac{1}{h(k, \Delta t)} = -c\Delta t + O(\Delta t^2) = O(\Delta t) \quad (25)$$

Therefore, G_h^2 proves to be more efficient than other methods in computing fast-scale cyclotron motions in long-term calculations.

The derivation process outlined above can be succinctly interpreted to mean that the Boris algorithm and G_h^2 converge towards the singularities of $h(k, \Delta t)$ at distinct values of k , corresponding respectively to the first term $(\frac{2\tan\frac{\theta}{2}}{\Delta t})^{-1}$ and the second term $(\frac{2\tan\frac{\theta - k\Delta t}{2}}{\Delta t})^{-1}$ of $h(k, \Delta t)$. The same analytical procedure can be replicated for λ_3 .

Until now, our theoretical investigations have successfully identified the most efficient numerical schemes for generating slow-scale guiding center motions (the Boris algorithm) and fast-scale cyclotron motions (G_h^2) among the spectrum of volume-preserving algorithms delineated by equations (12). Numerical experiments and comparisons between the Boris algorithm and G_h^2 will be conducted in the next section. The explicit expression of their corresponding rotation matrix R_B and $R_{G_h^2}$ are given by

$$R_B = \frac{1}{4 + \theta_x^2} \begin{bmatrix} 4 + \theta_x^2 - \theta_y^2 - \theta_z^2 & 2\theta_x\theta_y + 4\theta_z & 2\theta_x\theta_z - 4\theta_y \\ 2\theta_x\theta_y - 4\theta_z & 4 + \theta_y^2 - \theta_x^2 - \theta_z^2 & 2\theta_y\theta_z + 4\theta_x \\ 2\theta_x\theta_z + 4\theta_y & 2\theta_y\theta_z - 4\theta_x & 4 + \theta_z^2 - \theta_x^2 - \theta_y^2 \end{bmatrix} \quad (26.a)$$

$$R_{G_h^2} = \frac{1}{\theta^2} \begin{bmatrix} \theta_x^2 + (\theta_y^2 + \theta_z^2)\cos\theta & \theta_x\theta_y(1 - \cos\theta) + \theta_z\theta\sin\theta & \theta_x\theta_z(1 - \cos\theta) - \theta_y\theta\sin\theta \\ \theta_x\theta_y(1 - \cos\theta) - \theta_z\theta\sin\theta & \theta_y^2 + (\theta_x^2 + \theta_z^2)\cos\theta & \theta_y\theta_z(1 - \cos\theta) + \theta_x\theta\sin\theta \\ \theta_x\theta_z(1 - \cos\theta) + \theta_y\theta\sin\theta & \theta_y\theta_z(1 - \cos\theta) - \theta_x\theta\sin\theta & \theta_z^2 + (\theta_x^2 + \theta_y^2)\cos\theta \end{bmatrix} \quad (26.b)$$

Here

$$\theta = B\Delta t, \theta_x = B_x\Delta t, \theta_y = B_y\Delta t, \theta_z = B_z\Delta t \quad (26.c)$$

4 Numerical Experiments

In this section, we numerically test two representative volume-preserving algorithms (the Boris algorithm and G_h^2), and verify their properties in calculating fast and slow scale motions. The variables will no longer be normalized in the subsequent text. Instead, the time variables will be qualified by the gyro-frequency of an ion in a certain magnetic field $B_0 = 1T$

$$\omega_{c0} = \frac{eB_0}{m_i} = 9.57 \times 10^7 s^{-1} \quad (27)$$

We initially disregard the impact of the electric field, i.e. $\vec{E} = (0, 0, 0)^T$. Consider the motion of a single ion in a toroidal magnetic field with magnetic field strength on the magnetic axis $B_{axis} = 2T$, major radius $R_0 = 1.67m$, minor radius $a = 0.6m$, and the safety factor

$$q = 2.52\left(\frac{r}{a}\right)^2 - 0.16\left(\frac{r}{a}\right) + 0.86 \quad (28)$$

with $r = \sqrt{(\sqrt{x^2 + y^2} - R_0)^2 + z^2}$. These parameters can be referenced in [23]. The magnetic field in the toroidal coordinates (r, θ, ϕ) is expressed as $\vec{B} = B_\theta\vec{e}_\theta + B_\phi\vec{e}_\phi$ with

$$B_\phi = \frac{B_{axis}R_0}{R_0 + r\cos\theta}, B_\theta = \frac{rB_\phi}{qR_0} \quad (29)$$

To apply the volume-preserving algorithms, we transform the toroidal magnetic field \vec{B} into the Cartesian coordinates (x, y, z) which is

$$B_x = -B_\phi\sin\phi - B_\theta\sin\theta\cos\phi = -\frac{B_{axis}R_0y}{x^2 + y^2} - \frac{B_{axis}xz}{q(x^2 + y^2)} \quad (30.a)$$

$$B_y = B_\phi\cos\phi - B_\theta\sin\theta\sin\phi = \frac{B_{axis}R_0x}{x^2 + y^2} - \frac{B_{axis}yz}{q(x^2 + y^2)} \quad (30.b)$$

$$B_z = B_\theta\cos\theta = \frac{B_{axis}(\sqrt{x^2 + y^2} - R_0)}{q\sqrt{x^2 + y^2}} \quad (30.c)$$

Starting with the initial position $\vec{r}_0 = (R_0 + 0.25a, 0, 0)^T = (1.82m, 0, 0)^T$ and the initial velocity $\vec{v}_0 = (0, 2 \times 10^4 m/s, 2 \times 10^5 m/s)$, the projection of

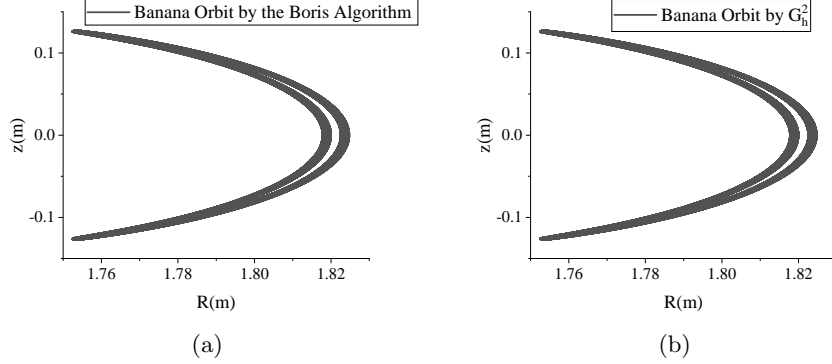


Figure 1: Numerical results with initial conditions of banana orbit. The time step size is $\omega_{c0}\Delta t = 0.1$, and the time integration interval is $[0, T_0]$ with $\omega_{c0}T_0 = 2.54 \times 10^4$ which is approximately one period of the slow-scale motions (banana period). The banana orbit is correctly obtained by both algorithms.

the particle's trajectory on the plane forms a closed banana orbit, and it will transform into a transit orbit when the initial velocity is changed into $\vec{v}_0 = (0, 8 \times 10^4 m/s, 2 \times 10^5 m/s)$. The Boris algorithm and G_h^2 are implemented with relatively large time step size $\omega_{c0}\Delta t = 0.1$, and the numerical results of the banana and transit orbit are shown in Figure 1 and Figure 2 respectively. The time integration interval is $[0, T_0]$, $\omega_{c0}T_0 = 2.54 \times 10^4$ for the banana orbit in Figure 1 and $[0, T_1]$, $\omega_{c0}T_1 = 1.38 \times 10^4$ for the transit orbit in Figure 2. Both algorithms have correctly achieved the trajectory of the trapped and transit particle due to their volume-preserving nature.

Now we analyze their differences by dividing the numerical solutions of position \vec{r} into two components: the slow-scale guiding center motions \vec{r}_G and the fast-scale cyclotron motions \vec{r}_C

$$\vec{r}_C = -\frac{m_i \vec{v} \times \vec{B}(\vec{r})}{e B^2(\vec{r})} \quad (31.a)$$

$$\vec{r}_G = \vec{r} - \vec{r}_C = \vec{r} + \frac{m_i \vec{v} \times \vec{B}(\vec{r})}{e B^2(\vec{r})} \quad (31.b)$$

Shown in Figure 3 and Figure 4 is the separated time-dependent numerical results of the banana orbit by both algorithms with $\omega_{c0}\Delta t = 0.1$ in selected time intervals of equal length of 10, together with the 'exact' solutions obtained by an extremely minuscule time step ($\omega_{c0}\Delta t = 10^{-4}$, which is virtually impossible to achieve in numerical simulations, and both algorithms generate identical results in this case. Here we select the result derived by the Boris algorithm). In Figure 3 we display the numerical and 'exact' results of the slow-scale motions \vec{r}_G . The Boris algorithm closely matches the analytical solution for slow-scale motions. In contrast, G_h^2 produces noticeable discrepancies, which are particularly evident

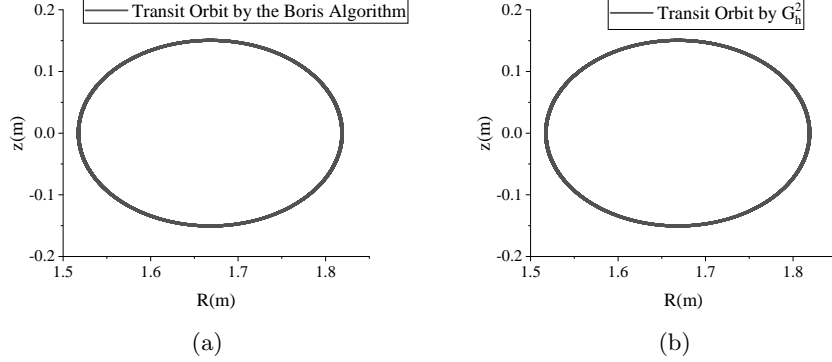


Figure 2: Numerical results with initial conditions of transit orbit. The time step size is $\omega_{c0}\Delta t = 0.1$, and the time integration interval is $[0, T_1]$ with $\omega_{c0}T_1 = 1.38 \times 10^4$ which is approximately one period of the slow-scale motions (transit period). The transit orbit is correctly obtained by both algorithms.

in Figure 3a and Figure 3b. Regarding the instances of the fast-scale motions \vec{r}_C depicted in Figure 4, the performances of the two algorithms are diametrically opposed: solutions derived from G_h^2 almost perfectly overlap with the analytical solution, and solutions of the Boris algorithm exhibit a significant phase error.

To test the efficiency of the two algorithms in handling diverse scales of motions, Figure 5 compares the global relative errors over the entire time integration interval $[0, T_0]$ of \vec{r}_G and \vec{r}_C as a function of time step size Δt . Here, the relative error is defined by

$$\epsilon_G = \frac{1}{N} \sum_{m=0}^{N-1} \sqrt{\frac{|\vec{r}_G^{exact}(t_m) - \vec{r}_G^{numerical}(t_m)|^2}{|\vec{r}_G^{exact}(t_m)|^2}} \quad (32.a)$$

$$\epsilon_C = \frac{1}{N} \sum_{m=0}^{N-1} \sqrt{\frac{|\vec{r}_C^{exact}(t_m) - \vec{r}_C^{numerical}(t_m)|^2}{|\vec{r}_C^{exact}(t_m)|^2}} \quad (32.b)$$

with $N = \frac{T_0}{\Delta t}$ the total number of time grids, and $t_m = (m + \frac{1}{2})\Delta t$ the corresponding time of the position variables in the m -th time step. It can be observed from Figure 5a that the relative error of Boris method converges faster in the case of slow-scale motions, while G_h^2 is more efficient in the fast-scale motions as shown in Figure 5b. The outcomes correspond to the phenomena illustrated in Figure 3 and Figure 4 respectively.

Now we compare the convergence rate of the DFT coefficients given by equation (13), which is measured by the 2-norm of errors between the numerical solutions and the "exact" solutions

$$\epsilon_\omega = \|\vec{f}^{exact}(\omega) - \vec{f}^{numerical}(\omega)\|_2 \quad (33)$$

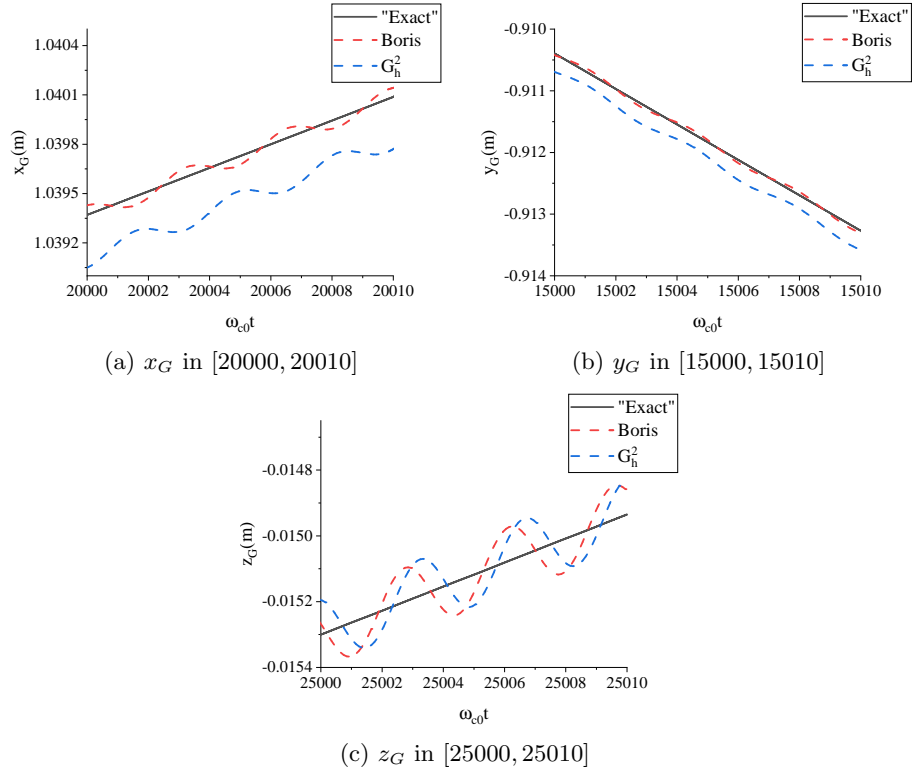


Figure 3: Time-dependent numerical and “exact” results of the slow-scale motions \vec{r}_G in certain time intervals. The red dashed lines (the Boris algorithm) oscillate closely around the black solid lines (“exact” solutions) in each graph. And the blue dashed lines (G_h^2) are significantly diverged from the black solid lines in (a) and (b).

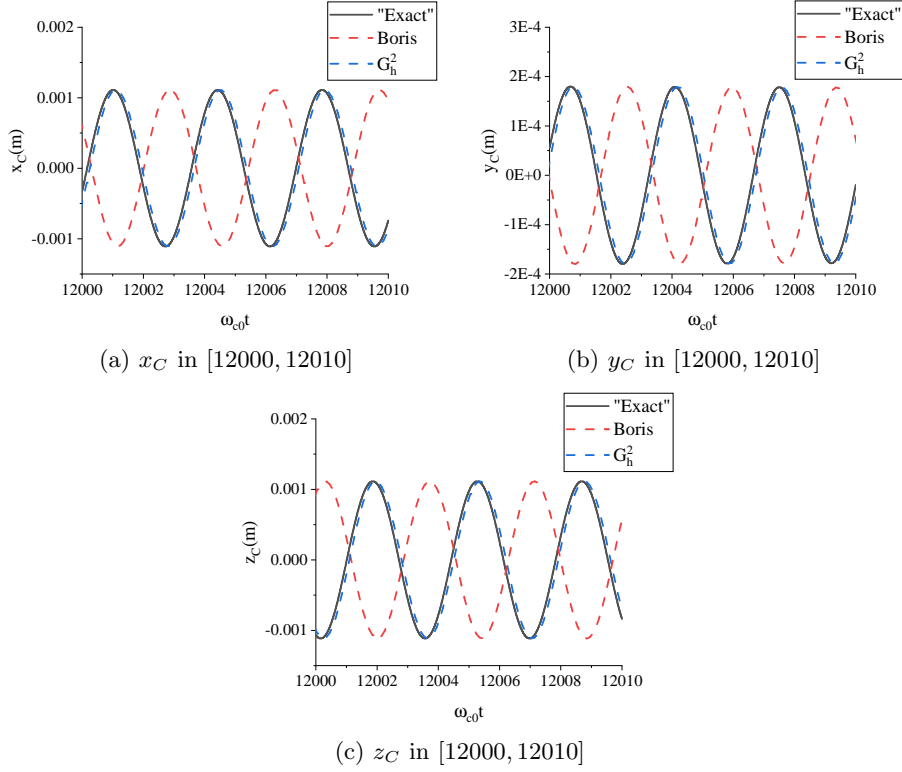


Figure 4: Time-dependent numerical and “exact” results of the fast-scale motions \vec{r}_C in certain time intervals. The blue dashed lines (G_h^2) almost overlap with the black solid lines (“exact” solutions), while the red dashed lines (the Boris algorithm) accumulate visible phase errors in each graph.

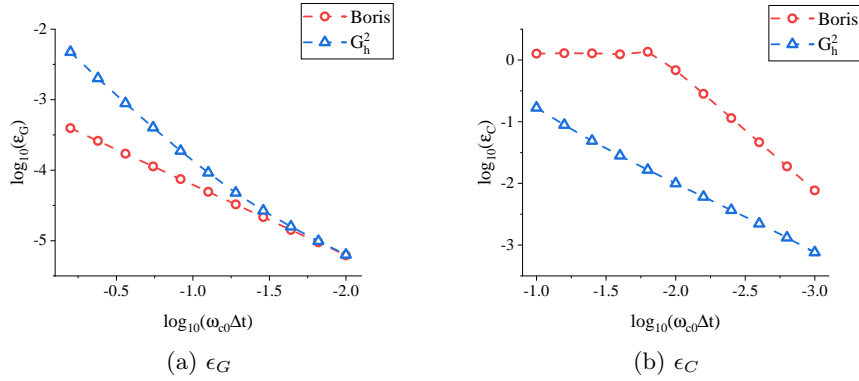


Figure 5: Global relative errors of \vec{r}_G and \vec{r}_C as a function of time step size Δt by both algorithms.

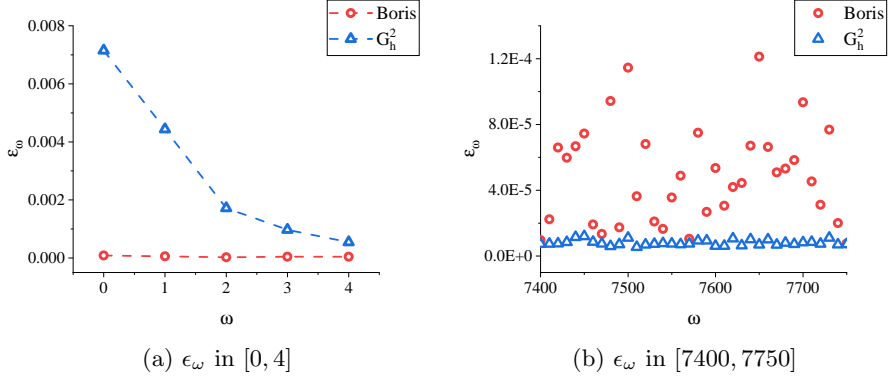


Figure 6: 2-norm errors of DFT coefficients ϵ_ω for various scales of ω .(a).small ω related to slow-scale guiding-center motions.(b).large ω related to fast-scale cyclotron motions

Figure 6a shows the results of small ω (i.e. $\omega \in [0, 4] \sim O(1)$, which reflects the slow-scale guiding center motions). The time step size is $\omega_{c0}\Delta t = 10^{-0.2}$ which is the largest size in Figure 5a. The outcomes of the Boris algorithm remain consistently similar to the "exact" cases while deviations are observed in the situations of G_h^2 . In the case of large ω (i.e. $\frac{2\pi\omega}{\omega_{c0}T} = \frac{B}{B_0} \sim O(1)$, which reflects the fast-scale cyclotron motions), the magnetic field strength B ranges from 1.84T to 1.92T over the entire banana period, resulting in non-trivial values of $\vec{f}(\omega)$ within the approximate range of [7400, 7750]. In Figure 6b we display the numerical errors with time step size $\omega_{c0}\Delta t = 0.1$ (which is the largest size in Figure 5b) and $\omega \in [7400, 7750]$, and the situation starkly contrasts with Figure 6a: the Boris algorithm yields completely distinct results to the "exact" solutions, with only minor errors occurring as for G_h^2 .

The above experiments corroborates the theoretical analysis of the preceding section: the guiding center orbit (slow-scale motions, low-frequency component of position) become more accurate utilizing the Boris algorithm, while the gyromotion (fast-scale motions, high-frequency component of position) is better described by G_h^2 due to the different convergence rate of the corresponding DFT coefficients.

Finally, we examine the process of wave heating by introducing a resonant electric field on the z-axis $\vec{E} = (0, 0, E_0 \cos(\omega_0 t))$, $E_0 = 5 \times 10^3 V/m$ with frequency ω_0 . The velocity magnitude v_k and relative error of kinetic energy ϵ_k in the k -th time step are calculated to quantify the impact of heating

$$v_k = |\vec{v}_k|, \epsilon_k = \frac{(v_k^{Exact})^2 - (v_k^{Numerical})^2}{(v_k^{Exact})^2} \quad (34)$$

Firstly, we consider the trapped particle with the same initial condition of banana orbit, and the frequency of the electric field ω_0 is set to be $\omega_0 = \frac{B(\vec{r})}{B_0} \omega_{c0}$ to match the gyro-frequency. The simulation over $[0, T_2]$ with $\omega_{c0}T_2 = 3 \times 10^3$

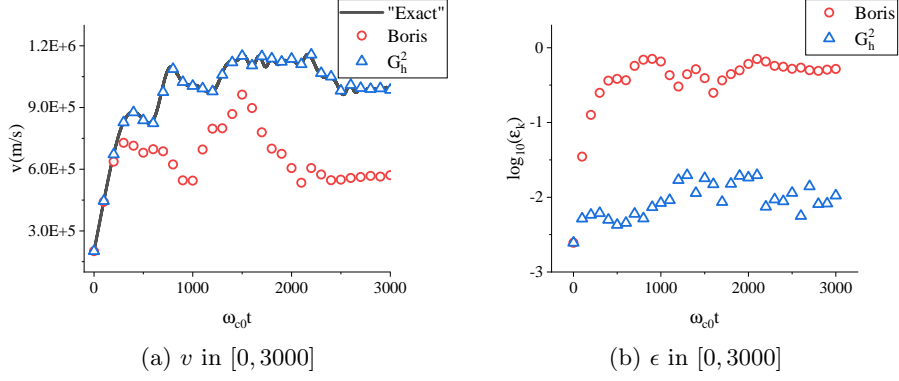


Figure 7: Numerical results of the trapped particle with an additional resonant electric field at the gyro-frequency and fixed time step size $\omega_{c0}\Delta t = 0.1$. The time integration interval is $[0, T_2]$, $\omega_{c0}T_2 = 3 \times 10^3$. (a). velocity magnitude v as a function of time. (b). relative error of kinetic energy ϵ . The numerical errors of the Boris algorithm is much larger than G_h^2 in this problem.

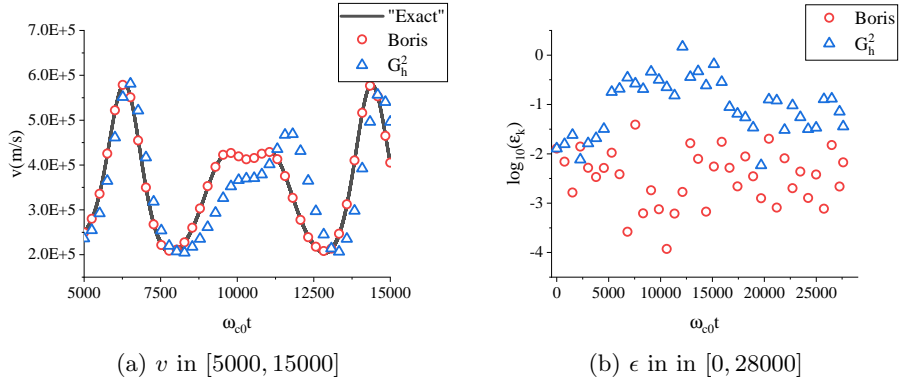


Figure 8: Numerical results of the transit particle with an additional resonant electric field at the transit frequency $\frac{2\pi}{T_1}$, $\omega_{c0}T_1 = 1.38 \times 10^4$ and fixed time step size $\omega_{c0}\Delta t = 10^{-0.2}$. The time integration interval is $[0, 2T_1]$. (a). velocity magnitude v in $[5000, 15000]$ as a function of time. (b). relative error of kinetic energy ϵ . The numerical errors of G_h^2 is much larger than the Boris algorithm in this problem.

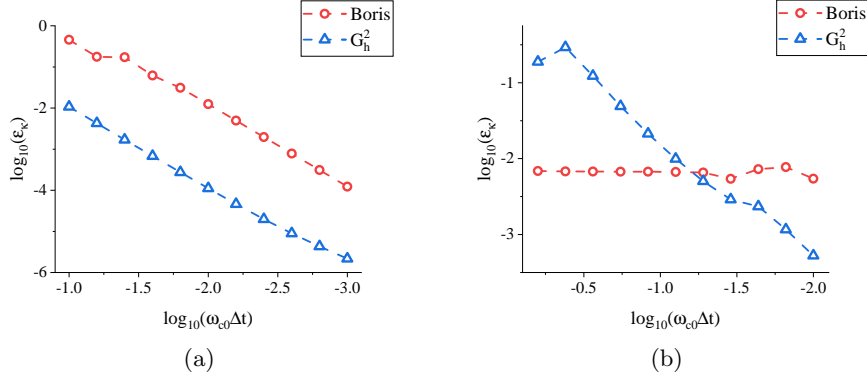


Figure 9: Global relative errors of kinetic energy ϵ_κ as a function of time step size Δt by both algorithms. (a). trapped particle with high-frequency resonant electric field. (b). transit particle with low-frequency resonant electric field.

and fixed time step size $\omega_{c0}\Delta t = 0.1$ is shown in Figure 7. In this case, G_h^2 provides superior numerical results compared to the Boris algorithm due to its higher accuracy of cyclotron motions. And shown in Figure 8 is the result of the transit particle with a low-frequency resonant electric field $\omega_0 = \frac{2\pi}{T_1}$ with $\omega_{c0}T_1 = 1.38 \times 10^4$ to match the transit period. The time step size is $\omega_{c0}\Delta t = 10^{-0.2}$, and the time integration interval is $[0, 2T_1]$. It is noticed that the Boris algorithm handles the low-frequency electric field better than G_h^2 in this example.

To analyze further, in Figure 9 we compute the global relative error of kinetic energy as a function of time step size Δt . Here, the global relative error ϵ_κ is defined by

$$\epsilon_\kappa = \frac{1}{N} \sum_{k=1}^N \epsilon_k \quad (35)$$

with $N = \frac{T_2}{\Delta t}$ or $N = \frac{2T_1}{\Delta t}$ the total number of time grids of the above two cases. For the case of high-frequency electric field in Figure 9a, both algorithms converge as the time step size diminished to zero, and G_h^2 allows for a significant larger time step size than the Boris algorithm (approximately one order of magnitude) to reach the same level of accuracy. The situation of low-frequency electric field in Figure 9b is slightly different. The precision of the Boris algorithm is virtually unaltered in the depicted range, while G_h^2 maintains the convergent numerical results. Nonetheless, the Boris algorithm still possesses substantial advantages at large time step sizes. One can observe that the two algorithms exhibit distinct advantages when addressing issues with varying characteristic frequencies, highlighting the importance of selecting the appropriate numerical scheme based on the specific motion scales or characteristic frequencies of interest.

5 Conclusion

In this study, we have conducted a comprehensive analysis of the efficacy of various volume-preserving algorithms in accurate single particle orbit simulations, particularly in context of the phase stability across various frequencies. Our findings, corroborated by both theoretical analysis and numerical experiments, consistently indicate that the Boris algorithm possesses superiority in simulating slow-scale guiding center motions, rendering it the optimal choice for physical problems characterized by low frequency scale, while G_h^2 have demonstrated enhanced efficiency in the simulation of fast-scale gyro-motions and high characteristic frequency. It is rather challenging to accurately calculate the guiding-center motion and gyro-motion simultaneously within the constraints of limited computational resources. Thus, the selection of the appropriate numerical scheme is pivotal and should be informed by the characteristic frequencies in specific physical problems of interest. For instance, for low frequency wave such as drift-wave turbulence and shear Alfvén waves, the Boris algorithm is typically the more favorable option. Conversely, for problems characterized by briefer time scales and high frequencies, such as RF heating, high frequency turbulence and ICE, G_h^2 may yield superior results.

Appendix: Approximation

We describe here the specific derivation process of equations (19) under the condition of approximation given by equation (16). Substituting equation (17.b) into (18) yields

$$\vec{f}(\omega) = \frac{\Delta t}{T} \exp\left(-\frac{1}{2}\Delta t \cdot i\right) (I_1 + I_2) \quad (A-1.a)$$

with

$$I_1 = \left(\vec{r}_0 + \frac{1}{2}\vec{v}_0\Delta t\right) \sum_{m=0}^{N-1} \exp(-km\Delta t \cdot i) \quad (A-1.b)$$

and

$$I_2 = \sum_{m=1}^{N-1} \sum_{j=1}^m \exp(-km\Delta t \cdot i) \vec{v}_j \Delta t \quad (A-1.c)$$

Since $\sum_{m=0}^{N-1} \exp(-km\Delta t \cdot i) = \frac{1-\exp(-kN\Delta t \cdot i)}{1-\exp(-k\Delta t \cdot i)} = \frac{1-\exp(-2\pi\omega \cdot i)}{1-\exp(-k\Delta t \cdot i)} = 0$, we have $I_1 = 0$. The simplification of I_2 is derived by exchanging the summation sequence

$$I_2 = \sum_{j=1}^{N-1} \sum_{m=j}^{N-1} \exp(-km\Delta t \cdot i) \vec{v}_j \Delta t = \frac{\Delta t}{1-\exp(-k\Delta t \cdot i)} \left(\sum_{j=1}^{N-1} \exp(-kj\Delta t \cdot i) \vec{v}_j - \sum_{j=1}^{N-1} \vec{v}_j \right) \quad (A-2)$$

By inserting the explicit formulation (17.a) for \vec{v}_j into the preceding equation, we derive the exact expressions for λ_1 , λ_2 , and λ_3

$$\lambda_1 = -N\Delta t = -T \quad (A-3.a)$$

$$\lambda_2 = \left(\sum_{j=1}^{N-1} \prod_{n=1}^j \mu_{2,n} - \sum_{j=1}^{N-1} \prod_{n=1}^j \lambda_{2,n} \right) \Delta t \quad (A-3.b)$$

$$\lambda_3 = \left(\sum_{j=1}^{N-1} \prod_{n=1}^j \mu_{3,n} - \sum_{j=1}^{N-1} \prod_{n=1}^j \lambda_{3,n} \right) \Delta t \quad (A-3.c)$$

with

$$\mu_{2,n} = \lambda_{2,n} \exp(-k\Delta t \cdot i), \mu_{3,n} = \lambda_{3,n} \exp(-k\Delta t \cdot i) \quad (A-3.d)$$

Now we are in the position to conduct approximations. We focus our analysis solely on λ_2 ; an identical process can be similarly applied to λ_3 , yielding analogous results. We henceforth substitute all subscripts n with $N-n$

$$\lambda_2 = \left(\sum_{j=1}^{N-1} \prod_{n=1}^j \mu_{2,N-n} - \sum_{j=1}^{N-1} \prod_{n=1}^j \lambda_{2,N-n} \right) \Delta t \quad (A-4)$$

This will facilitate the formulation of λ_2 in a recursive manner

$$a_n = (1 + a_{n-1})\lambda_{2,n}, a_1 = \lambda_{2,1}; b_n = (1 + b_{n-1})\mu_{2,n}, b_1 = \mu_{2,1} \quad (A-5.a)$$

and

$$\lambda_2 = (b_{N-1} - a_{N-1})\Delta t \quad (A-5.b)$$

Similarly, we shall first concentrate on a_n . Before delving into the asymptotic behavior of a_n , we shall initially elucidate the interrelation between $\lambda_{2,n}$ and $\lambda_{2,n+1}$ utilizing equation (16)

$$\lambda_{2,n+1} = \lambda_{2,n} \exp(-\Delta B_n \Delta t \cdot i) = \lambda_{2,n} \exp(O(\epsilon^{1+\alpha} \Delta t)) \quad (A-6)$$

Setting $\lambda_{2,0} = \lambda_{2,1}$, the approximation of a_n is determined by

$$a_n = \frac{\lambda_{2,n}}{1 - \lambda_{2,n}} \left(1 - \prod_{m=0}^{n-1} \lambda_{2,m} \right) + (n-1)O(\epsilon^{1+\alpha} \Delta t) \quad (A-7)$$

We now employ mathematical induction to substantiate this conclusion. For $n=1$, $a_1 = \lambda_{2,1} = \frac{\lambda_{2,1}}{1 - \lambda_{2,1}}(1 - \lambda_{2,0})$ is trivial. Supposing that the aforementioned approximation is valid for n ; hence, for the case of $n+1$, by recurrence relations

in equation (A-5.a) we obtain

$$\begin{aligned}
a_{n+1} &= (1 + a_n)\lambda_{2,n+1} \\
&= \left(1 + \frac{\lambda_{2,n} - \prod_{m=0}^n \lambda_{2,m}}{1 - \lambda_{2,n}} + (n-1)O(\epsilon^{1+\alpha}\Delta t)\right)\lambda_{2,n+1} \\
&= \frac{\lambda_{2,n+1}}{1 - \lambda_{2,n+1}} \left(1 - \prod_{m=0}^n \lambda_{2,m}\right) + \lambda_{2,n+1} \left(1 - \prod_{m=0}^n \lambda_{2,m}\right) \left(\frac{1}{1 - \lambda_{2,n}} - \frac{1}{1 - \lambda_{2,n+1}}\right) \\
&\quad + (n-1)O(\epsilon^{1+\alpha}\Delta t)\lambda_{2,n+1}
\end{aligned}$$

Since $|\lambda_{2,m}| = 1$ holds for arbitrary m , we have $\lambda_{2,n+1}(1 - \prod_{m=0}^n \lambda_{2,m}) = O(1)$ and $(n-1)O(\epsilon^{1+\alpha}\Delta t)\lambda_{2,n+1} = (n-1)O(\epsilon^{1+\alpha}\Delta t)$. The remaining term $\left(\frac{1}{1 - \lambda_{2,n}} - \frac{1}{1 - \lambda_{2,n+1}}\right)$ can be reduced to

$$\frac{1}{1 - \lambda_{2n}} - \frac{1}{1 - \lambda_{2,n+1}} = \left(\frac{1}{2\tan\frac{\theta_n}{2}} - \frac{1}{2\tan\frac{\theta_n + O(\epsilon^{1+\alpha}\Delta t)}{2}}\right) \cdot i = O(\epsilon^{1+\alpha}\Delta t) \quad (A-8)$$

Integrating the preceding equations yields

$$a_{n+1} = \frac{\lambda_{2,n+1}}{1 - \lambda_{2,n+1}} \left(1 - \prod_{m=0}^n \lambda_{2,m}\right) + n \cdot O(\epsilon^{1+\alpha}\Delta t) \quad (A-9)$$

Thus the above proof is concluded. The estimation for b_n yields an identical conclusion

$$b_n = \frac{\mu_{2,n}}{1 - \mu_{2,n}} \left(1 - \prod_{m=0}^{n-1} \mu_{2,m}\right) + (n-1)O(\epsilon^{1+\alpha}\Delta t) \quad (A-10)$$

To attain a structure akin to equation (19), it is imperative to fulfill the subsequent conditions

$$(N-1)O(\epsilon^{1+\alpha}\Delta t) = O\left(\frac{T}{\Delta t} \cdot \epsilon^{1+\alpha}\Delta t\right) = O(\epsilon^\alpha) \quad (A-11)$$

and

$$\prod_{m=0}^{N-1} \mu_{2,m} = \prod_{m=0}^{N-1} \lambda_{2,m} \exp(-k\Delta t \cdot i) = \left(\prod_{m=0}^{N-1} \lambda_{2,m}\right) \cdot \exp(-kN\Delta t \cdot i) = \prod_{m=0}^{N-1} \lambda_{2,m} \quad (A-12)$$

Combining equations (A-5.b),(A-7),(A-10),(A-11) and (A-12), the approximation of λ_2 is finally derived

$$\begin{aligned}\lambda_2 &= \left(\sum_{j=1}^{N-1} \prod_{n=1}^j \mu_{2,N-n} - \sum_{j=1}^{N-1} \prod_{n=1}^j \lambda_{2,N-n} \right) \Delta t \\ &= \left[\left(1 - \prod_{m=0}^{N-2} \lambda_{2,m} \right) \left(\frac{\mu_{2,N-1}}{1 - \mu_{2,N-1}} - \frac{\lambda_{2,N-1}}{1 - \lambda_{2,N-1}} \right) + O(\epsilon^\alpha) \right] \Delta t \\ &= \left[\left(1 - \prod_{m=0}^{N-2} \lambda_{2,m} \right) \left(\frac{\lambda_{2,N-1} \exp(-k\Delta t \cdot i)}{1 - \lambda_{2,N-1} \exp(-k\Delta t \cdot i)} - \frac{\lambda_{2,N-1}}{1 - \lambda_{2,N-1}} \right) + O(\epsilon^\alpha) \right] \Delta t\end{aligned}$$

which is identical to equation (19.c) by replacing n with $N - n$ in $\lambda_{2,n}$, as previously stated in (A-4).

Acknowledgments

J.W. thanks Zehua Qian and Youjun Hu for useful discussions. This work was supported by the National Natural Science Foundation of China under Grant No. 12205339.

References

- [1] Yang Chen and Scott E. Parker. “A δf particle method for gyrokinetic simulations with kinetic electrons and electromagnetic perturbations”. In: *Journal of Computational Physics* 189.2 (2003), pp. 463–475. ISSN: 0021-9991. DOI: [https://doi.org/10.1016/S0021-9991\(03\)00228-6](https://doi.org/10.1016/S0021-9991(03)00228-6). URL: <https://www.sciencedirect.com/science/article/pii/S0021999103002286>.
- [2] E. Lanti et al. “Orb5: A global electromagnetic gyrokinetic code using the PIC approach in toroidal geometry”. In: *Computer Physics Communications* 251 (2020), p. 107072. ISSN: 0010-4655. DOI: <https://doi.org/10.1016/j.cpc.2019.107072>. URL: <https://www.sciencedirect.com/science/article/pii/S0010465519303911>.
- [3] V. Grandgirard et al. “GYSELA, a full-f global gyrokinetic Semi-Lagrangian code for ITG turbulence simulations”. In: *AIP Conference Proceedings* 871.1 (Nov. 2006), pp. 100–111. ISSN: 0094-243X. DOI: 10.1063/1.2404543. eprint: https://pubs.aip.org/aip/acp/article-pdf/871/1/100/11637840/100_1_1_online.pdf. URL: <https://doi.org/10.1063/1.2404543>.
- [4] A. J. Brizard and T. S. Hahm. “Foundations of nonlinear gyrokinetic theory”. In: *Rev. Mod. Phys.* 79 (2 Apr. 2007), pp. 421–468. DOI: 10.1103/RevModPhys.79.421. URL: <https://link.aps.org/doi/10.1103/RevModPhys.79.421>.

- [5] Animesh Kuley et al. “Verification of particle simulation of radio frequency waves in fusion plasmas”. In: *Physics of Plasmas* 20.10 (Oct. 2013), p. 102515. ISSN: 1070-664X. DOI: 10.1063/1.4826507. eprint: https://pubs.aip.org/aip/pop/article-pdf/doi/10.1063/1.4826507/15683930/102515\1\1_online.pdf. URL: <https://doi.org/10.1063/1.4826507>.
- [6] A. Kuley et al. “Verification of nonlinear particle simulation of radio frequency waves in tokamak”. In: *Physics of Plasmas* 22.10 (Oct. 2015), p. 102515. ISSN: 1070-664X. DOI: 10.1063/1.4934606. eprint: https://pubs.aip.org/aip/pop/article-pdf/doi/10.1063/1.4934606/13531306/102515\1\1_online.pdf. URL: <https://doi.org/10.1063/1.4934606>.
- [7] M. Raeth and K. Hallatschek. “High-Frequency Nongyrokinetic Turbulence at Tokamak Edge Parameters”. In: *Phys. Rev. Lett.* 133 (19 Nov. 2024), p. 195101. DOI: 10.1103/PhysRevLett.133.195101. URL: <https://link.aps.org/doi/10.1103/PhysRevLett.133.195101>.
- [8] Y. Y. Yu et al. “Verification of a fully kinetic ion model for electromagnetic simulations of high-frequency waves in toroidal geometry”. In: *Physics of Plasmas* 29.7 (July 2022), p. 073902. ISSN: 1070-664X. DOI: 10.1063/5.0090168. eprint: https://pubs.aip.org/aip/pop/article-pdf/doi/10.1063/5.0090168/16593804/073902\1\1_online.pdf. URL: <https://doi.org/10.1063/5.0090168>.
- [9] Yang Chen and Scott E. Parker. “Particle-in-cell simulation with Vlasov ions and drift kinetic electrons”. In: *Physics of Plasmas* 16.5 (May 2009), p. 052305. ISSN: 1070-664X. DOI: 10.1063/1.3138743. eprint: https://pubs.aip.org/aip/pop/article-pdf/doi/10.1063/1.3138743/14026699/052305\1\1_online.pdf. URL: <https://doi.org/10.1063/1.3138743>.
- [10] Y Lin et al. “An improved gyrokinetic electron and fully kinetic ion particle simulation scheme: benchmark with a linear tearing mode”. In: *Plasma Physics and Controlled Fusion* 53.5 (Apr. 2011), p. 054013. DOI: 10.1088/0741-3335/53/5/054013. URL: <https://dx.doi.org/10.1088/0741-3335/53/5/054013>.
- [11] Jay P. Boris and Ramy A. Shanny. “Proceedings, Fourth Conference on the Numerical Simulation of Plasmas : November 2, 3, 1970, Naval Research Laboratory, Washington, D.C.” In: 1971. URL: <https://api.semanticscholar.org/CorpusID:107199562>.
- [12] R.W. Hockney and J.W. Eastwood. *Computer Simulation Using Particles*. 1st ed. CRC Press, 1988. URL: <https://doi.org/10.1201/9780367806934>.
- [13] C.K. Birdsall and A.B Langdon. *Plasma Physics via Computer Simulation*. 1st ed. CRC Press, 1991. URL: <https://doi.org/10.1201/9781315275048>.

- [14] S.E Parker and C.K Birdsall. “Numerical error in electron orbits with large $\omega_{ce}\Delta t$ ”. In: *Journal of Computational Physics* 97.1 (1991), pp. 91–102. ISSN: 0021-9991. DOI: [https://doi.org/10.1016/0021-9991\(91\)90040-R](https://doi.org/10.1016/0021-9991(91)90040-R). URL: <https://www.sciencedirect.com/science/article/pii/S002199919190040R>.
- [15] P. H. Stoltz et al. “Efficiency of a Boris-like integration scheme with spatial stepping”. In: *Phys. Rev. ST Accel. Beams* 5 (9 Sept. 2002), p. 094001. DOI: 10.1103/PhysRevSTAB.5.094001. URL: <https://link.aps.org/doi/10.1103/PhysRevSTAB.5.094001>.
- [16] G Penn et al. “Boris push with spatial stepping”. In: *Journal of Physics G: Nuclear and Particle Physics* 29.8 (July 2003), p. 1719. DOI: 10.1088/0954-3899/29/8/337. URL: <https://dx.doi.org/10.1088/0954-3899/29/8/337>.
- [17] Hong Qin et al. “Why is Boris algorithm so good?” In: *Physics of Plasmas* 20.8 (Aug. 2013), p. 084503. ISSN: 1070-664X. DOI: 10.1063/1.4818428. eprint: https://pubs.aip.org/aip/pop/article-pdf/doi/10.1063/1.4818428/16059300/084503_1_online.pdf. URL: <https://doi.org/10.1063/1.4818428>.
- [18] Ruili Zhang et al. “Application of Lie Algebra in Constructing Volume-Preserving Algorithms for Charged Particles Dynamics”. In: *Communications in Computational Physics* 19.5 (2016), pp. 1397–1408. DOI: 10.4208/cicp.scpde14.33s.
- [19] Yang He et al. “Volume-preserving algorithms for charged particle dynamics”. In: *Journal of Computational Physics* 281 (2015), pp. 135–147. ISSN: 0021-9991. DOI: <https://doi.org/10.1016/j.jcp.2014.10.032>. URL: <https://www.sciencedirect.com/science/article/pii/S0021999114007141>.
- [20] Yang He et al. “Higher order volume-preserving schemes for charged particle dynamics”. In: *Journal of Computational Physics* 305 (2016), pp. 172–184. ISSN: 0021-9991. DOI: <https://doi.org/10.1016/j.jcp.2015.10.032>. URL: <https://www.sciencedirect.com/science/article/pii/S0021999115007081>.
- [21] Yang He et al. “High order volume-preserving algorithms for relativistic charged particles in general electromagnetic fields”. In: *Physics of Plasmas (1994-present)* 23 (Aug. 2016). DOI: 10.1063/1.4962677.
- [22] Yulei Wang, Hong Qin, and Jian Liu. “Multi-scale full-orbit analysis on phase-space behavior of runaway electrons in tokamak fields with synchrotron radiation”. In: *Physics of Plasmas* 23.6 (June 2016), p. 062505. ISSN: 1070-664X. DOI: 10.1063/1.4953608. eprint: https://pubs.aip.org/aip/pop/article-pdf/doi/10.1063/1.4953608/15907421/062505_1_online.pdf. URL: <https://doi.org/10.1063/1.4953608>.

- [23] T. Görler et al. “Intercode comparison of gyrokinetic global electromagnetic modes”. In: *Physics of Plasmas* 23.7 (July 2016), p. 072503. ISSN: 1070-664X. DOI: 10.1063/1.4954915. eprint: https://pubs.aip.org/aip/pop/article-pdf/doi/10.1063/1.4954915/14129468/072503_1_online.pdf. URL: <https://doi.org/10.1063/1.4954915>.
- [24] V. Grandgirard et al. “A 5D gyrokinetic full-f global semi-lagrangian code for flux-driven ion turbulence simulations”. In: *Computer Physics Communications* 207 (2016), pp. 35–68. DOI: 10.1016/j.cpc.2016.05.007. URL: <http://dx.doi.org/10.1016/j.cpc.2016.05.007>.
- [25] Yu Lin et al. “A gyrokinetic electron and fully kinetic ion plasma simulation model”. In: *Plasma Physics and Controlled Fusion* 47.4 (Mar. 2005), p. 657. DOI: 10.1088/0741-3335/47/4/006. URL: <https://dx.doi.org/10.1088/0741-3335/47/4/006>.
- [26] Youjun Hu et al. “Fully Kinetic Simulation of Ion-Temperature-Gradient Instabilities in Tokamaks”. In: *Plasma* 1.1 (2018), pp. 105–118. ISSN: 2571-6182. DOI: 10.3390/plasma1010010. URL: <https://www.mdpi.com/2571-6182/1/1/10>.
- [27] T. J. Bogaarts et al. “Development and application of a hybrid MHD-kinetic model in JOREK”. In: *Physics of Plasmas* 29.12 (Dec. 2022), p. 122501. ISSN: 1070-664X. DOI: 10.1063/5.0119435. eprint: https://pubs.aip.org/aip/pop/article-pdf/doi/10.1063/5.0119435/16778964/122501_1_online.pdf. URL: <https://doi.org/10.1063/5.0119435>.
- [28] Alex Friedman et al. “Multi-scale particle-in-cell plasma simulation”. In: *Journal of Computational Physics* 96 (1991), pp. 54–70. URL: <https://api.semanticscholar.org/CorpusID:122845298>.
- [29] O Buneman. “Time-reversible difference procedures”. In: *Journal of Computational Physics* 1.4 (1967), pp. 517–535. ISSN: 0021-9991. DOI: [https://doi.org/10.1016/0021-9991\(67\)90056-3](https://doi.org/10.1016/0021-9991(67)90056-3). URL: <https://www.sciencedirect.com/science/article/pii/0021999167900563>.
- [30] Ernst Hairer, Christian Lubich, and Bin Wang. “A filtered Boris algorithm for charged-particle dynamics in a strong magnetic field”. In: *Numerische Mathematik* 144.4 (Apr. 2020), pp. 787–809. ISSN: 0945-3245. DOI: 10.1007/s00211-020-01105-3. URL: <https://doi.org/10.1007/s00211-020-01105-3>.
- [31] Ernst Hairer and Christian Lubich. “Long-term analysis of a variational integrator for charged-particle dynamics in a strong magnetic field”. In: *Numerische Mathematik* 144.3 (Mar. 2020), pp. 699–728. ISSN: 0945-3245. DOI: 10.1007/s00211-019-01093-z. URL: <https://doi.org/10.1007/s00211-019-01093-z>.

- [32] Ernst Hairer, Christian Lubich, and Yanyan Shi. “Large-stepsize integrators for charged-particle dynamics over multiple time scales”. In: *Numerische Mathematik* 151.3 (July 2022), pp. 659–691. ISSN: 0945-3245. DOI: 10.1007/s00211-022-01298-9. URL: <https://doi.org/10.1007/s00211-022-01298-9>.